

Sub-100 mK Cooling Using Normal-Metal\Insulator\Superconductor Tunnel Junctions

Peter J. Lowell · Galen C. O'Neil ·
Jason M. Underwood · Xiaohang Zhang ·
Joel N. Ullom

Received: 12 July 2013 / Accepted: 6 December 2013
© Springer Science+Business Media, LLC (outside the USA) 2013

Abstract Normal-metal\insulator\superconductor (NIS) junctions can be used as solid-state refrigerators since the hottest electrons preferentially tunnel from the normal metal into the superconductor. In this paper, we present NIS junctions optimized to cool electrons from a bath temperature of 100 mK. We measure a temperature reduction of the electrons in the refrigerator junctions from 100 to 26 mK which agrees with device models. Independent measurements of the electron temperature using thermometer junctions measure a temperature decrease from 100 to 48 mK. Theories explaining the difference in measured temperatures are discussed.

Keywords Microrefrigerators · Electron cooling · Superconducting tunnel junctions

1 Introduction

Modern science often studies or exploits the quantum mechanical properties of condensed-matter systems. Sub-Kelvin temperatures are often required to make these quantum mechanical properties apparent. Temperatures as low as 300 mK can be reached simply by pumping on liquid ^3He , but reaching lower temperatures requires complex, expensive machinery such as dilution refrigerators (DRs) and adiabatic demagnetization refrigerators (ADRs). In order to increase the

Contribution of the US government; not subject to copyright in the United States.

P. J. Lowell (✉) · G. C. O'Neil · J. M. Underwood · X. Zhang · J. N. Ullom
National Institute of Standards and Technology, 325 Broadway MS 817.03,
Boulder, CO 80305, USA
e-mail: peter.lowell@nist.gov

J. N. Ullom
e-mail: joel.ullom@nist.gov

accessibility of temperatures below 300 mK, simpler and more cost effective refrigeration techniques are desirable. Solid-state refrigeration such as cooling by normal-metal\insulator\superconductor (NIS) junctions provides a simpler alternative to these more conventional methods. In the past, NIS junctions have been shown to cool electrons [1–4], bulk objects [5] and lithographically integrated superconducting detectors [6]. Recently, NIS junctions have been used to cool a suspended copper cold plate to which a user can attach arbitrary payloads from 290 to 256 mK [7], and using this technique, cooling to temperatures close to 100 mK is predicted. A general-purpose NIS refrigerator, backed by a pumped ³He bath, would offer a lower-cost route to temperatures near 100 mK. Even lower temperatures are desirable, however, and multi-stage NIS refrigerators could provide temperature reductions from 300 mK to less than 50 mK. To achieve this goal, we present measurements of NIS junctions designed to cool electrons from 100 mK to base temperatures below 50 mK.

2 Theory

NIS junctions can be used as a refrigerator since, when a junction is biased near the superconducting gap, the hottest electrons preferentially tunnel from the normal metal into the superconductor, transferring heat in the process. According to the Bardeen–Cooper–Schrieffer (BCS) theory of superconductivity, the current through a biased NIS junction is given by

$$I_{NIS} = \frac{1}{eR_n} \int_0^\infty [f_N(E - eV_b) - f_N(E + eV_b)] \frac{|E - i\Gamma|}{\sqrt{(E - i\Gamma)^2 - \Delta^2}} dE \quad (1)$$

where e is the electron charge, R_n is the normal state resistance of the junction, $f_{N,S}$ is the Fermi function in the normal metal (superconductor), Γ is the Dynes parameter, a phenomenological parameter used to describe the presence of subgap states, and Δ is the gap of the superconductor. Equation 1 shows that the current through an NIS junction only depends on the device parameters R_n , Γ and Δ and the temperature of the normal metal. Therefore, with an accurate knowledge of R_n , Γ and Δ , NIS junctions can also be used to measure the temperature of the electron system in the normal metal. The cooling power of the junction can be determined by multiplying the current by the energy transferred from the normal metal into the superconductor as

$$P_N = \frac{1}{e^2 R_n} \int_{-\infty}^\infty (E - eV_b) [f_S(E) - f_N(E - eV_b)] \frac{|E - i\Gamma|}{\sqrt{(E - i\Gamma)^2 - \Delta^2}} dE \quad (2)$$

where a negative power indicates power being removed from the normal metal. The minimum temperature of the base electrode occurs when the cooling power of the refrigerator equals the power load from the environment:

$$P_N(T_N, T_S) + \beta P_S(T_N, T_S) + \Sigma(T_b)\Omega \left(T_p^{n(T_b)} - T_e^{n(T_b)} \right) + I_2 V_b + I^2 R_{pad} = 0, \quad (3)$$

where $T_{N,S,b}$ are the normal-metal, superconductor and bath temperatures, Σ is the electron–phonon coupling constant, and Ω is the normal-metal volume. The βP_S term represents a heat inflow from the superconducting electrode. This is modeled as a percentage of the power deposited into the superconductor, $P_S = P_N + IV$, returning to the normal metal. The value of β can be calculated using methods described in O’Neil et al. [4]. The $\Sigma(T_b)\Omega \left(T_p^{n(T_b)} - T_e^{n(T_b)} \right)$ term describes the power deposited due to the hot phonons in the lattice interacting with the electrons in the normal metal through the electron–phonon coupling. We have measured the T dependence of Σ and n for our devices [8]. The I_2V term represents a power load from two-particle tunneling due to Andreev reflections [9]. Finally, the I^2R_{pad} term represents Joule heating due to the resistance of the normal metal. We used Eq. 3 to design optimized devices and found that we could improve our cooling over previous devices by increasing the normal-metal thickness and the junction aspect ratio to reduce Joule heating in the normal-metal pad and by increasing the resistance of the refrigerator junction to increase the junction quality.

3 Experimental Methods and Results

Figure 1 shows a representative NIS refrigerator used in this paper. The electrons in the normal metal are cooled by two $3 \mu\text{m} \times 32 \mu\text{m}$ refrigerator junctions. According to Eq. 2, the cooling power of an NIS junction scales inversely with junction resistance. Thus, if one wishes to use an NIS junction as a thermometer (cf. Eq. 1), the junction resistance must be sufficiently high or the bias must be sufficiently low to avoid self-cooling errors. We measured the electron temperature in the base electrode by extending the normal-metal film to a pair of smaller ($3 \mu\text{m} \times 5 \mu\text{m}$), NIS junctions that have a thicker junction oxide and negligible cooling power.

The devices were fabricated on a Si wafer with 150 nm of thermally grown SiO_2 . The normal-metal base electrode, a 46 nm AlMn (4,000 ppm at% Mn) film, was deposited with DC magnetron sputtering. This layer was then patterned

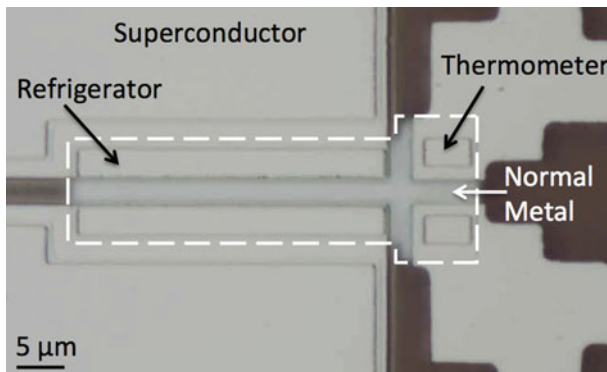


Fig. 1 Photograph of our NIS device. The electrons in the normal metal, outlined, are cooled by the refrigerator junctions and the temperature is measured using the thermometer junctions. (Color figure online)

using standard photo-lithographic techniques and wet etched in a heated acid bath. Next, the base electrode was passivated under 150 nm of SiO₂ deposited by plasma-enhanced chemical vapor deposition to protect it from future processing steps. The thermometer junction area was defined by plasma etching vias in the SiO₂. The wafer was then ion-milled to remove any surface contaminants and then exposed to a linear ramp of O₂ to 50 Torr over 15 min and then was allowed to oxidize for 30 min for a total dose of 110,000 Torr s to make junctions with a resistance area product, $R_{SP} \equiv R \times A$, of about 5,900 $\Omega \mu\text{m}^2$. Using DC magnetron sputtering, 300 nm of Al was deposited, patterned and acid etched to complete the thermometer junctions. Once the thermometer junctions were completed, vias were opened in the SiO₂ using a plasma etch to define the refrigerator junctions. The wafer was then ion-milled and exposed to 2,900 Torr s of O₂ and capped with 430 nm of Al to form junctions with a R_{SP} of 2,200 $\Omega \mu\text{m}^2$. To improve the cooling performance of the refrigerator junctions, we then oxidized the Al with 0.3 Torr s of O₂ and deposited 450 nm of AlMn (4,000 ppm at% Mn) to form a quasiparticle trap [4]. The refrigerator junctions were completed by patterning and etching the wafer in a heated acid bath.

Devices were measured in an ADR with a base temperature of about 60 mK. Small excess power loads due to RF pick-up can greatly affect the cooling properties of the junctions, as we have observed in previous experiments. This pick-up has a larger effect at lower temperatures, so much more care must be taken to reduce pick-up than in our previous experiments. All measurement lines were filtered at 300 K, 4 K and at 60 mK with commercial low-pass filters. To further reduce the power loads, we blackened all of the inside surfaces of the sample box and covered all mating surfaces of the sample box and cryostat light shields with Al tape. We also increased the shielding of all room temperature wires by enclosing them in braided tinned copper sheaths. We observed that these precautions greatly reduced the pick-up in our devices, allowing us to measure temperature sensitivity in the IV characteristics of our junctions at lower temperatures.

Measurements of the junctions were performed by supplying a bias current from a low-noise voltage source in series with a known bias resistor. Voltage signals across the junctions were amplified using low-noise room temperature amplifiers. The resistances of the junctions were determined by comparing the IV characteristics of the junctions above voltage biases of $4\Delta/e$ to IV curves generated using BCS theory. The Dynes parameter Γ is determined from the ratio of the normal state to the sub-gap resistance. The superconducting gap Δ is determined by a least-squares minimization between the temperature derived from IV curves and the cryostat temperature, which was calibrated to a calibrated Johnson noise thermometer.

The cooling experiment was performed by biasing the refrigerator junctions with the current that produces the maximum cooling and then measuring the electron temperature of the normal metal with the thermometer junctions. The refrigerator bias that produces the maximum cooling, called the optimal bias, is found by maximizing the potential difference across a thermometer junction which is biased with alternating

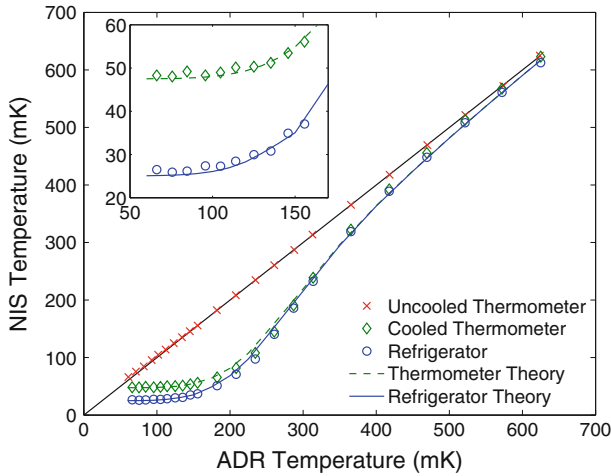


Fig. 2 Temperature of the normal-metal base electrode, T_N , versus ADR temperature as measured by the thermometer and refrigerator junctions. The *solid black line* shows where the normal-metal temperature equals the bath temperature, which represents no heating or cooling. The measured temperature from the thermometer junctions, the red X's, is in good agreement with the calibrated Johnson noise thermometer. The cooled electrons in the refrigerator junctions, the *blue circles*, are in good agreement with our model, calculated using Eq. 3 using measured device parameters, $\beta = 0.014$ and 40 fW of stray power, represented by the *blue line*. The cooled electron temperature in the normal metal measured by independent thermometers is represented by the *green diamonds*. The *green dashed* theory curve is calculated using the same model as the *blue curve*, but with an additional 1.4 pW of stray power. This temperature reduction in the separate thermometer is an improvement over previous devices [4]. *Inset* zoomed view for temperatures from 50 to 150 mK. (Color figure online)

positive and negative currents to compensate for voltage offsets and drift. To obtain a more accurate measurement of the cooled electron temperature, we then supply the optimal bias to the refrigerator junctions and measure the IV characteristics of the thermometer junction. To convert this IV curve to a temperature, we compare this curve to a family of IV curves generated from BCS theory for a variety of temperatures. We then use an interpolation routine to find the temperature of every IV point in the measured curve. By taking IV curves of the refrigerator junctions versus temperature to obtain Δ , Γ and R_n , we were also able to measure the temperature from the refrigerator IV curves using the same method.

The main results of this paper are shown in Fig. 2, where the electron temperature in the normal metal is plotted versus the ADR bath temperature. To determine how well the thermometer junctions performed, we compared their uncooled temperature to the calibrated cryostat temperature. Figure 2 shows that the uncooled thermometer junctions agree with the ADR temperature from 60 to 600 mK. The agreement over this temperature range is an improvement over previous devices and we believe that this shows that we were successful in reducing RF pick-up. Using the thermometer junctions to measure the electron temperature in the cooled normal metal, we measure an electron temperature reduction from 100 to 48 mK and from 150 to 55 mK, an improvement over previous devices optimized to cool from 300 mK. Another, independent, measurement of the normal-metal electron temperature is provided by the IV

characteristics of the refrigerator junctions. As Fig. 2 shows, the measured electron temperature in the refrigerator junctions is in good agreement with the temperature of the thermometer junctions for temperatures above about 250 mK. However, the two temperature measurements start to deviate for temperatures below 250 mK. When the refrigerator IV curves are the source of the temperature measurement, we observe that the electrons inside of the refrigerator junctions are cooled from 100 to 26 mK.

Stray power loads deposited directly into the thermometer junctions can heat up the thermometer, possibly explaining our observed divergence in temperatures. At lower temperatures, the uncooled thermometer temperature starts to deviate from the ADR temperature by a few milliKelvin. The power required to raise the temperature of the normal metal by this amount can be calculated using Eq. 3. The observed temperature difference between the uncooled thermometer and the ADR temperature corresponds to a power load of under 40 fW. Using Eq. 3, we were able to model the cooling performance of the refrigerators using device parameters of $R_N = 23 \Omega$, $\Delta = 185.7 \mu\text{eV}$, $\Gamma = 4.6 \times 10^{-8} \text{ eV}$, $\Omega = 10.7 \mu\text{m}^3$, $R_{pad} = 0.14 \Omega$, a β value of 0.014, and 40 fW of stray power. The calculated theory agrees with our measured data. To explain the temperature measurements of the cooled thermometer junctions, we must add an additional 1.4 pW of stray power to our model. This is much more than the 40 fW of stray power we inferred previously. It is important to note that this line also represents the temperature reduction provided by one junction with 1.4 pW of science load, or about 3 pW for the pair. Other effects including an athermal electron distribution in the normal metal may be able to explain the temperature discrepancy between the refrigerator and thermometer junctions. We are currently investigating these ideas further. However, by reducing the stray RF power in our cryostat, we were able to significantly reduce this discrepancy from previous devices [4].

4 Conclusions

We have designed and fabricated NIS devices optimized for cooling from temperatures near 100 mK. Measurements of the electron temperature in the refrigerator junctions agrees with device modeling and show cooling from 100 to 26 mK. However, in nearby thermometer junctions, we measure cooling of electrons from 100 to 48 mK and from 150 to 55 mK. As with previous devices, we observe a disagreement between the refrigerator and thermometer electron temperatures and are currently investigating this discrepancy. Improved RF filtering has reduced this disagreement from earlier work.

Acknowledgments This work is supported by the NASA APRA program.

References

1. M. Nahum, T. Eiles, J. Martinis, Appl. Phys. Lett. **65**, 3123–3125 (1994)
2. P.J. Koppinen, I.J. Maasilta, Phys. Rev. Lett. **102**, 165502 (2009)
3. H. Nguyen, L. Pascal, Z. Peng, O. Buisson, B. Gilles, C. Winkelmann, H. Courtois, Appl. Phys. Lett. **100**, 252602 (2012)
4. G.C. O’Neil, P.J. Lowell, J.M. Underwood, J.N. Ullom, Phys. Rev B **85**, 134504 (2012)

5. A. Clark, N. Miller, A. Williams, S. Ruggiero, G. Hilton, L. Vale, J. Beall, K. Irwin, J. Ullom, *Appl. Phys. Lett.* **86**, 173508 (2005)
6. N. Miller, G. O'Neil, J. Beall, G. Hilton, K. Irwin, D. Schmidt, L. Vale, J. Ullom, *Appl. Phys. Lett.* **92**, 163501 (2008)
7. P.J. Lowell, G.C. O'Neil, J.M. Underwood, J.N. Ullom, *Appl. Phys. Lett.* **102**, 082601 (2013)
8. J.M. Underwood, P.J. Lowell, G.C. O'Neil, J.N. Ullom, *Phys. Rev. Lett.* **107**, 255504 (2011)
9. S. Rajauria, P. Gandit, T. Fournier, F.W.J. Hekking, B. Pannetier, H. Courtois, *Phys. Rev. Lett.* **100**, 207002 (2008)